Electronic Supplementary Material (ESI) for Physical Chemistry Chemical Physics.
This journal is © the Owner Societies 2022

Insights into the impact of photophysical processes and defect state evolution on the emission properties of surface-modified ZnO nanoplates for application in photocatalysis and hybrid LEDs

*Dhritiman Banerjee[1] *, Payal Banerjee[2], Asit Kumar Kar[1]*

[1]Micro and Nano Science Laboratory, Department of Physics, Indian Institute of Technology (Indian School of Mines), Dhanbad, Jharkhand, 826004, India

[2] Department of Chemistry, National Tsing Hua University, Hsinchu, 300044, Taiwan (R.O.C.)

***Corresponding author:** banerjeegora90@gmail.com*

S1. Structural study of crystalline pure and surface-modified ZnO

S1.1. XRD spectra analysis.

The structural property of the pure crystalline ZnO and on capping with polymers PVA and PMMA has been studied using X-ray diffraction (XRD) spectroscopy. The crystal structure analysis of the pure and surface-modified ZnO samples was carried out by X-ray diffractometer using Cu Kα radiation. The diffractogram was recorded in the 2θ range from 10° to 80° with a step size of 0.01313°. The XRD diffractogram for the pure and surface-modified ZnO samples are shown in Figure. S1 (a). The XRD diffractogram has prominent peaks[1] at 31.6°, 34.2°, 36.1°, 47.3°, 56.3°, 62.7°, 66.2°, 67.5° and 68.8° which belong to (100), (002), (101), (102), (110), (103), (200), (112) and (201) crystal planes respectively. The peaks match well with the [2]JCPDS file no. 036-1451 and no impurity peaks were observed, which confirmed the formation of pure hexagonal wurtzite zinc oxide crystals. The observed prominent peaks, i.e. (100) and (002), confirm the good crystallinity of all the prepared samples. The peak at 31.6° corresponds to (100) slip plane direction represented as $[2\bar{1}\bar{1}0]$ in the ZnO crystal. The suppression of the (002) plane on modifying the surface of ZnO by polymers confirms the suppression of growth and orientation of the ZnO crystal along the c-axis. In the case of the ZnO samples modified using PMMA polymer, higher capping of growth of nanocrystals took place that is evident from the decrease in intensity (100), (002) and (101) crystal planes.

The crystallite size of the ZnO powders for ZnO, ZPVA3 and ZPMMA3 samples prepared by direct precipitation method was determined from the broadening of the X-ray diffraction peaks using the Scherer formula:

$$D = \frac{0.89\lambda}{\beta cos\theta} \qquad (1)$$

In this equation (1), wavelength λ of Cu k_α radiation is 1.54 Å, β is the full width at half maximum of the peak, and θ is the Bragg's angle obtained from the 2θ value corresponding to the maximum intensity peak in the XRD spectrum.

The crystallite size obtained for ZnO, ZPVA3 and ZPMMA3 samples is *15.8 nm, 13.5 nm and 13.2 nm*, respectively. A decrease in crystallite size confirms the suppression of the growth of crystallites on polymer capping.

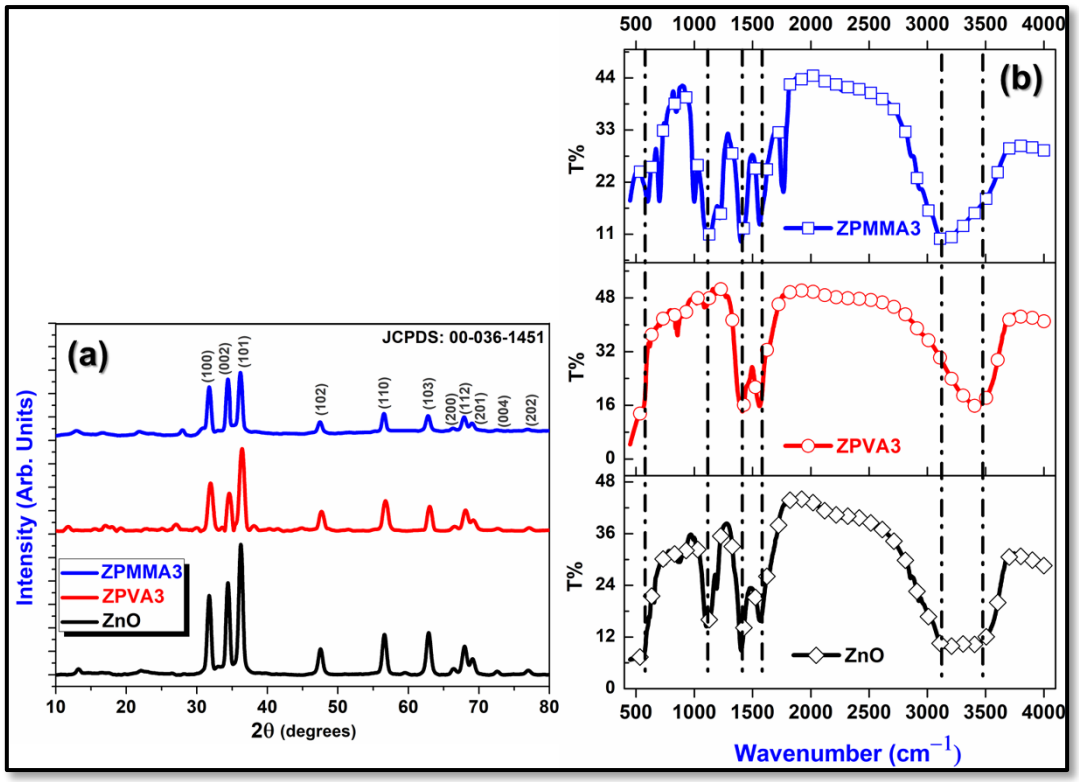

Figure. S1 (a) XRD diffractogram pattern of pure ZnO, surface modified ZnO samples using polymer PVA (ZPVA3) and PMMA (ZPMMA3), (b) FTIR spectra of pure ZnO, surface modified ZnO using polymer PVA (ZPVA3) and PMMA (ZPMMA3).

S1.2. Infrared spectra Analysis.

FTIR spectra as shown in Figure. S1 (b) represents the spectra for pure ZnO and surface-modified ZnO using polymers PVA or PMMA. It was studied to identify the nature and type of vibrational bond in ZnO and surface-modified ZnO samples. The peak at 584 cm^{-1} is assigned to the Zn-O bond[3]. The peak at 1120 cm^{-1} corresponds to –OH group bonded by hydrogen bond in the metal oxide ZnO[4], which is heavily suppressed in ZPVA3 spectra indicating that in PVA functional group[5] interaction with hydroxide group present on the surface of ZnO. In the ZPMMA3 sample, the peaks at 1022 cm^{-1} and 1340 cm^{-1} are assigned to [6]complex formation between COO^- groups[7] with Zn ions. This attachment between a metal oxide and carboxylate ion[8] is considered to be weak generally. They may bind through 3 types of bind mode [9,10.11], namely- (1) mono-dentate ester type, (2) bi-dentate chelating, and (3) bi-dentate bridging. The peak at 3442 cm^{-1} represents –OH stretching in ZnO[12] and ZPVA3 samples while the peak disappears in ZPMMA3 samples, which means this –OH stretching[13] is suppressed on modifying ZnO surface with PMMA which binds to ZnO using carbonyl group. The band at 3145.9 cm^{-1} proved the presence of −OH groups on the ZnO surface[14]. The 1766 cm^{-1} is the characteristics[15,16] ester carbonyl −C=O stretch vibration of PMMA. The peak at 1404 cm^{-1} present in every sample corresponds to symmetric stretching frequencies of the carboxylate group in the precursor[17]. Asymmetric stretching frequencies of the carboxylate group in the precursor are observed[18] at 1604 cm^{-1} and 1543 cm^{-1}. In the case of ZPVA3 samples, the bond for –OH gets shifted by $\nabla\upsilon$ = 300 cm^{-1} w.r.t. ZnO pure sample. The band of surface –OH group shifted in the case of ZPMMA3 too. This shifting further confirms the interaction between ZnO NPs and the polymer.

The frequency of vibrations are calculated considering the system has been attached to a spring with spring constant k and reduced mass μ using the formula:

$$\upsilon = \frac{1}{2\pi c}\sqrt{\frac{k}{\mu}} \quad (2)$$

The equation's significance is that a change in the functional group changes the frequency of vibration of the system directly, according to equation 2. The different functional groups give rise to a different vibration frequency due to differences in their reduced masses. This leads to the shifting of the frequency of vibration in the FTIR spectra.

S1.3. Mechanism behind the growth of ZnO nanoplates: The concentration of hydroxide ions at which the ZnO nanopowders were synthesized is responsible for the growth of pure ZnO nanoplates. At the used hydroxide ions concentration in the precursor, many hydroxide ions remained unused in the reaction that gets adsorbed on the c-axis, i.e., polar [0001] plane of ZnO. The adsorption of hydroxide ions on the polar surface retards the growth of the [0001] plane and promotes the growth along $[01\bar{1}0]$ and $[2\bar{1}\bar{1}0]$ non-polar planes as shown in the Figure. 1 (g) in the manuscript, which leads to the growth of the nano-plate structures, consistent with the XRD analysis where we observed (002) and (100) planes the signature peaks of the nanoplate structure. Suppression of the (002) plane on polymer-based surface modification confirms the disorientation of the nanoplate structures. In the case of the growth of ZnO nanoplates in polymer PMMA and PVA, the growth along the c-axis is further prohibited by the polymer as the functional group interacts with the ZnO polar (0001) plane found in the FTIR studies. The change in −OH stretching peak in the case of surface-modified samples confirms that both −OH and polymer can suppress the growth along the c-axis and promote the growth of ZnO nanoplates.

S1.4. Interaction of ZnO with PVA and PMMA

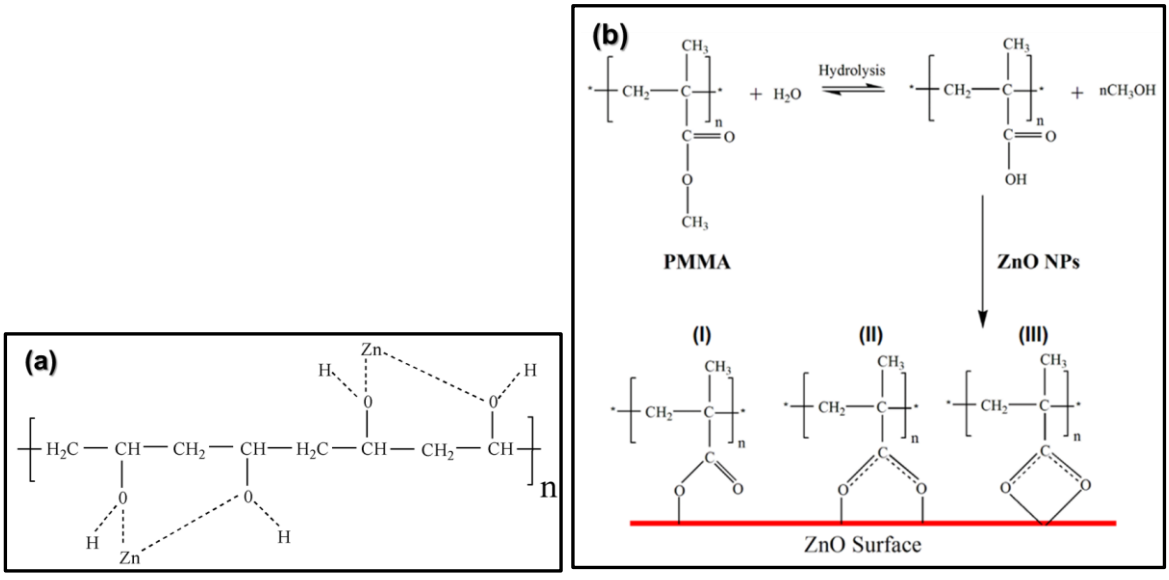

Figure. S2 (a) Schematic illustration of the chemical structure of ZnO capped by PVA showing metal cations bonded with the PVA polymer chains through hydrogen bonding, (b) Chemical structure and reaction scheme for the formation of ZnO capped by PMMA polymer through three types of binding: (I) mono-dentate ester type, (II) bi-dentate chelating, and (III) bi-dentate bridging between –COOH group and the ZnO surface.

S2. Bandgap and Urbach tail energy values of pure and surface-modified ZnO

- **Bandgap calculation {Tauc Plot}**

Tauc relation is used to calculate the optical band gap of the material as given below:

$$(\alpha h\nu) = A(h\nu - E_g)^{\boldsymbol{n}} \qquad (3)$$

In the above relation, E_g is the optical band gap of the material; A is a constant, $h\nu$ represents the energy of the photon, $n = \frac{1}{2}$ for direct allowed transition and $n = 2$ for indirectly allowed transitions. So, the band gap for direct band gap material is determined by extrapolating the linear portion of the curve obtained by plotting $(\alpha h\nu)^2$ vs hν. In our samples, the value of n used was as $n = \frac{1}{2}$ as ZnO is a direct band gap transition material.

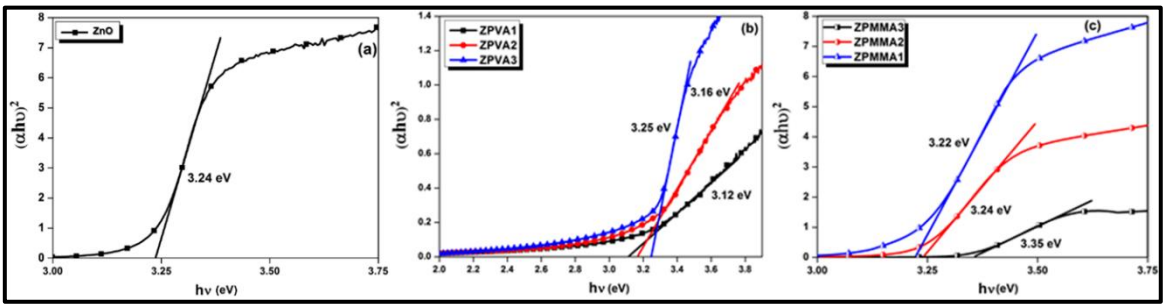

Figure. S3 Tauc plots of ZnO samples (a) pure ZnO, (b) Surface-modified using PVA, (c) Surface-modified using PMMA.

The band gaps are found to increase with a decrease in oxygen vacancy calculated using XPS spectra, details of which are given in table 1 in section 3.3.1. of the manuscript. ZnO has the highest oxygen vacancy, followed by ZPVA3 and ZPMMA3 samples calculated from O(1s) spectra [V_O − ZnO>ZPVA3>ZPMMA3]. The band gap follows the order ZnO<ZPVA3<ZPMMA3, i.e., with the increase in oxygen vacancy band gap decreases. This phenomenon is known as oxygen vacancy induced band gap narrowing[19, 20].

- **Urbach tail energy**

In semiconductors, the absorption edge increases exponentially below the band edge absorption known as Urbach tail energy. Excitons, phonons, and structural disorders have been pointed out to be the reason behind the presence of this tail in the relevant literature. The greater the value of Urbach tail energy greater is the value of structural disorder in the sample. But the striking feature to note here is that only the samples ZPMMA2 and ZPMMA3 have Urbach energy less than the value of pure ZnO samples. Still, the emission intensity of all the surface-modified samples is less than that of the pure ZnO sample, thus revealing that rather than chemical structural modification, some physical interactions between the ZnO and the polymer might have a bigger role behind luminescence from ZnO nanoplates. The Urbach tail energy has been calculated using the equation (4) given below for analyzing spectral dependence of the absorption edge:

$$\alpha\ (\upsilon) = \alpha_0 \exp\left(\frac{h\upsilon}{E_U}\right) \qquad (4)$$

The equation represents an optical transition between the occupied states in the valence band tail and unoccupied states in the conduction band edge.

Table S1. Experimental band gap (*Eg*) and Urbach energy (E_U) values of pure and surface-modified ZnO nanoplate samples.

Sample name	*Band gap (eV)*	*Urbach energy (E_U) (meV)*
1. ZnO	3.24	158
2. ZPVA1	3.12	821
3. ZPVA2	3.16	613
4. ZPVA3	3.25	297
5. ZPMMA1	3.22	181
6. ZPMMA2	3.24	149
7. ZPMMA3	3.35	95

S3. Details of Photoluminescence spectra peak fitting

Table S2. The output of Gaussian peak fitting of photoluminescence emission spectra of ZnO, ZPVA3 and ZPMMA3 samples

ZnO *Peak Position (nm)*	*Width nm*	*ZPVA3* *Peak Position (nm)*	*Width nm*	*ZPMMA3* *Peak Position (nm)*	*Width nm*
1. 345.34703	11.12223	329.93404	16.23213	370.78809	8.09591
2. 366.04008	39.5444	367.27213	44.29627	380.26142	12.91072
3. 398.2964	27.71762	405.03278	22.48013	394.05699	18.31096
4. 428.84033	34.25521	422.28064	13.41035	412.23236	15.59633
5. 458.32013	21.97265	438.19184	21.24877	425.94074	10.66943
6. 469.63758	10.90782	470.21673	32.52552	435.70877	25.2823
7. 484.28813	9.42369	510.75816	63.02574	457.15176	11.409
8. 504.88269	22.35078	528.68284	40.14262	467.30126	8.52735
9. 529.92896	14.5929	577.51046	24.33436	474.29629	5.80587
10. 550.73893	21.78294	608.44304	15.80325	483.1769	13.34819
11. 585.00527	32.37167	658.81233	67.63143	498.00373	6.81128
12. 597.65842	101.02521	x	x	507.87627	8.92255
13. 663.32764	750.04731	x	x	x	x
14. 668.82212	0.05078	x	x	x	x

The deconvolution of the PL spectra was done by analysing the possible origin of individual components made from the available energy positions of various defect centres existing within the Zn–O system. The best fit resulted from the fitting the PL spectra of ZnO, ZPVA3 and ZPMMA3 as shown in fig. 6 (a), (b), and (c) in the main manuscript using Gaussian function, which converges after multiple iterations with maximum reduced chi-square value and R^2 value approaching close to unity resulting in the overlap between the cumulative fitted curve and the experimental curve.

Table S3. Integrated intensity ratios of defect states and UV emission from pure and surface-modified ZnO

Samples	I_V/I_{UV}	I_B/I_{UV}	I_G/I_{UV}	$I_{Y/O}/I_{UV}$	I_R/I_{UV}
ZnO	1.52	1.68	0.53	1.53	0.27
ZPVA3	0.9	0.47	0.42	0.052	0.12
ZPMMA3	0.89	0.40	0.07	×	×

As surface modification reduces defect state density, we need to calculate the percentage decrease in the defect state density in surface-modified ZnO nanoplates compared to pure ZnO nanoplates. It has been calculated by comparing the percentage decrease in emission w.r.t. pure ZnO nanoparticles for various emission states, which has been given in the Table S4.

Table S4. Percentage decrease in defect states w.r.t. to ZnO nanoplates calculated from Gaussian fitting of PL spectra

Samples	**UV**	**Violet**	**Blue**	**Green**	**Yellow**	**Red**
Defect states	***Free exciton***	***Zn_i***	***Ext. Zn_i***	***V_O***	***O_i***	***Excess O***
ZPVA3	21.7	53.3	79.6	81.03	97.4	64.1
ZPMMA3	21.6	54.2	81.2	96.87	100	100

S4. Förster resonance energy transfer (FRET) calculation and Charge Transfer (CT)

S4.1. FRET process

- Förster resonance energy transfer (FRET) is a type of non-radiative energy transfer between the donor and the acceptor through dipole-dipole interaction. FRET is a distance-dependent energy transfer mechanism between two molecules, which are approximated to be point dipoles. Since the excited donor loses its excitation to the acceptor by the coupling of transition dipoles, it is a nonradiative loss process. In our system, i.e., surface modified ZnO samples, the photogenerated excitons (Wannier) are formed inside the excited donor ZnO molecules, while the large concentration of charge carriers presents in the excited energy states of the polymer (surface-modifying polymers, e.g., PVA and PMMA) acts as an acceptor. The process of energy transfer becomes more and more efficient with the greater overlap between the emission spectra of the donor and the absorption spectra of the acceptor. In the original FRET theory first developed by Förster, he assumed that the relative position and orientation of the dipoles are fixed, which is not valid in our case as the excitons formed inside our donor sample is mobile, and they are surrounded by a large concentration of acceptor charge carriers in the polymers. Therefore, we have modified our calculation to explain our system, and thus we need to consider two different cases:

  (i) Point to point dipole approximation.

  (ii) Interaction within the plane of donor and acceptor as FRET process is affected by the geometrical distribution of donors and acceptors.

The process can be represented by the following process, where the asterisk mark (*/**) represents the excited state.

$$ZnO + h\nu = (ZnO)^{**} \quad (5)$$

$$(ZnO)^{**} + Polymer = (ZnO)^{*} + (Polymer)^{*} \quad (6)$$

$$(ZnO)^{*} = ZnO + h\nu' \text{ (radiative)} \quad (7)$$

$$(Polymer)^{*} = (Polymer) + h\nu'' \text{ (non-radiative)} \quad (8)$$

Also, the location inside the particle from where the energy is transferred to the polymer must not exceed the FRET limit, i.e., 1-10 nm.

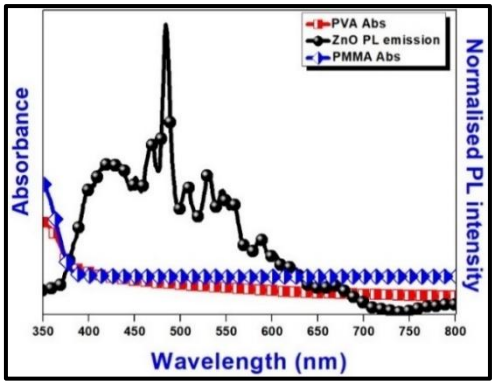

Figure. S4 Spectral overlaps of the ZnO nanoparticles emission with the absorption spectra of polymers PVA and PMMA.

So, based on standard FRET theory developed by Förster, we will try to calculate various FRET parameters such as the efficiency of energy transfer (E), Förster radius (R_0) and the actual distance between the donor (ZnO) and acceptor capping agent.

As per FRET theory proposed by Förster, the energy transfer efficiency can be calculated from experimental donor emission profile by the equation:

$$E = 1 - \frac{I'}{I} \qquad (9)$$

Where, I' and I are the total normalized fluorescence (PL) emission intensities of the donor with and without acceptor (A). Using the obtained energy value from equation (9) in equation (10), we get the relation between R and R_0. The energy transfer efficiency equation can also be expressed in terms of Förster radius (R_0) and the actual distance between donor-acceptor (R) as:

$$E = \frac{R_0^6}{R_0^6 + R^6} \qquad (10)$$

Where R_0 is known as Förster radius, i.e., the distance at which the donor can transfer half of the excitation energy to the acceptor. This can be calculated using the equation:

$$R_0 = 0.211 \times (\kappa^2 \eta^{-4} Y_D J)^{\frac{1}{6}} \text{ Å} \qquad (11)$$

Å=Unit of length angstrom.

Where, κ^2 =Angular orientation between acceptor and donor dipoles = $\frac{2}{3}$

η = Refractive index of ZnO = 2.013

Y_D = Quantum yield of ZnO = 0.122

J = Spectral overlap integral of the donor-acceptor pairs

$$\text{J}(\lambda) = \sum_a^b F(\lambda)\varepsilon(\lambda)\lambda^4 . \qquad (12)$$

J is the spectral overlap integral in between donor fluorescence emission spectrum (F (λ) is the normalized fluorescence spectrum of the donor), and acceptor absorption spectrum (scaled by its molar extinction coefficient, ε) given here in terms of wavelength λ (in units of nm). The calculated numerical values of J for ZnO modified

using PVA and PMMA using equation (12) are 1.45×10^{14}, and 4.99×10^{12} respectively. Using the value of R_0 obtained from equation (11) in equation (10) we get the distance between donor and acceptor FRET pain, i.e., *R*.

S4.2. Charge transfer (CT) process

Adsorption of oxygen on the surface or grain boundaries in ZnO takes place in the dark by directly capturing electrons from the surface, leading to the formation of a superoxide charge transfer ($CT_{O_2^-}$) state in the middle of the energy band gap. When the sample is excited under UV light, photogenerated holes are captured by these superoxides[21,22], leading to the release of trapped electrons to the conduction band that brings down band bending by neutralizing the ionized oxygen vacancies present on the surface.

$$O_2 + e^- \longrightarrow O_2^- \quad \text{[In dark]} \qquad (13)$$

$$O_2^- + h^+ \longrightarrow O_2 + e^- \quad \text{[Under UV]} \qquad (14)$$

A part of the photoexcited holes is also transferred to the polymer's energy levels, which reduces band bending near the surface of ZnO due to the generation of ionized oxygen vacancies. Therefore, two ways charge carrier transfer take place from the surface of ZnO to oxygen molecule generation the superoxide charge transfer state or by direct transfer of photoexcited holes from the ZnO NPs to the polymer. The cumulative effect of these two processes determines the emission of green colour[23,30] and other emissions from ZnO energy states.

$$V_o^0 \longrightarrow V_o^+ + e^- \qquad (15)$$

$$V_o^+ \longrightarrow V_o^{++} + e^- \qquad (16)$$

$$V_o^{++} + h^+ \longrightarrow h\nu_{green} \qquad (17)$$

$$V_o^+ + e^- \longrightarrow V_o^0 \qquad (18)$$

The released electron e^- according to equation (14) increases the concentration of available free electrons, which will raise the electron quasi-Fermi level, which means most of the time, the oxygen vacancy (V_O) will exist in a neutral state (V_o^0) according to equation (18). The singly ionized oxygen vacancy V_o^+ is passivated by the release of a trapped electron by the oxygen at the grain boundary. Also, on capping with polymers, the surface states appear to get modified as the holes instead of getting trapped at the surface, move/transfer to the HOMO of the polymers so the trapped electron could not radiatively recombine with the polymers photogenerated hole to give green emission according to equation (17). The entire process of FRET and CT have been represented in energy diagram S5.

S4.3. Energy Band Diagram

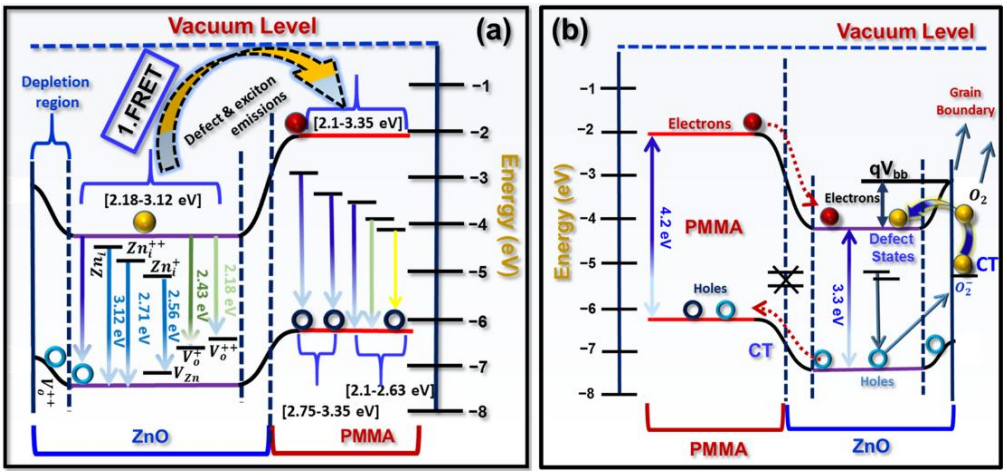

Figure. S5 Energy diagram representing quenching of emission from excitonic and defect states through (a) FRET and (b) Charge transfer (CT) in between ZnO[24,25] and PMMA[26].

S5. The mechanism behind UV and orange-red emission

S5.1. The mechanism behind enhanced UV emission from ZnO on capping

Another important observation in all the spectra that can be made is that UV emission enhances with quenching of green luminescence in capped ZnO nanoparticles. This observation has been attributed to increased electron-hole radiative recombination on suppression of green emission in surface-modified ZnO. The presence of shallow surface traps or dark excitons arising from fine structure splitting[27,28] may explain UV emission peaks at the nanometre scale. The red shifting of band edge emission observed in pure ZnO sample contrary to expected band edge emission of ZnO in the range 350 nm-400 nm can be ascribed to oxygen vacancy induced red shifting of the band gap of ZnO as discussed in section 3.2.1. in the manuscript.

S5.2. Origin of orange-red emission in uncapped and capped ZnO

The orange-red emission[29] has a particular pattern in all the samples of ZnO modified by the polymer. It has been observed in the Figure. 3 of the manuscript, all the samples with a reasonable amount of green emission. Orange-red emission peaks rise and fall with green luminescence peaks. As the polymers, PVA and PMMA have sufficient oxygen atoms in their functional group, it saturates the surface of the ZnO nanoparticles with excess oxygen. But when these oxygen atoms fail to find the exact position for binding on the ZnO surface, then a defect complex is generated on the surface of the ZnO. These defect complexes generated due to excess oxygen on the surface of the ZnO are generally regarded as the driving factor behind orange-red emission in ZnO. The quenched red emission in ZPMMA3 confirms that excess oxygen adsorption is not the cause of green emission quenching. So, the reason is the presence of photophysical pathways potent enough to quench the emission.

S5.3. Green emission in pure and surface-modified ZnO NPs

Photoluminescence emission spectra can be a way forward in understanding what type of oxygen vacancy dominates the ZnO and the surface-modified ZnO. This is possible because if V_O^+ captures an electron from the CB to generate neutral oxygen vacancy (V_o) from where the transition to VB takes place to give green emission[30] at 500 nm. On the other hand, if V_O^+ captures a hole it will generate V_O^{++}state where if an electron recombines from the conduction band to emit 565 nm wavelength.

$$V_o \longleftrightarrow V_O^+ + e^- \qquad (19)$$

$$V_O^{++} \longleftrightarrow V_O^+ + h^+ \qquad (20)$$

The reaction (19) takes place in the bulk region, while (20) takes place in the depletion region of the ZnO[31]. The holes are not trapped in the PMMA modified ZnO as discussed previously, because of which the emission at 550 nm is completely suppressed. So, V_O^{++} the state is expected to be absent in the PMMA modified ZnO nanoparticles as 550 nm emission is completely suppressed in the ZPMMA3 sample.

S6. CIE colour chromaticity

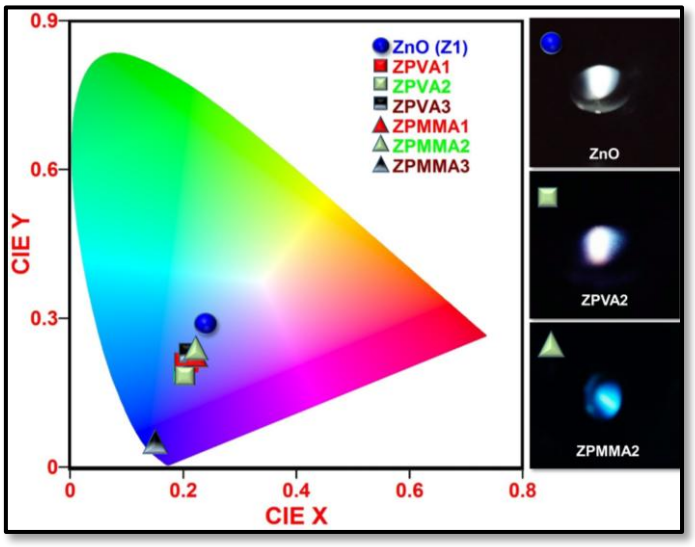

Figure S6. CIE chromaticity coordinates and digital photographs of emitting pure and surface-modified ZnO NPs.

S7. Modification in band bending due to surface modification

On surface modification of ZnO NPs with a polymer such as PVA, or PMMA, the polymers will reduce the chance of hole trapping and formation of V_0^{++} recombination centre. As the chance of creation of V_0^{++} recombination centre gets reduced on surface modification there will be a sharp reduction in band bending leading to the rise of V_0^{+}/V_0^{++} energy levels above Fermi level. This will lead to the suppression of green emission from surface-modified ZnO NPs by reducing the surface-induced band bending effect.

The whole process has been modelled mathematically and presented here.

The width of band bending W can be calculated using the formula:

$$W = \left[\frac{2K_{ZnO/ZnO-polymer}\, V_{bb}}{eN_D}\right]^{\frac{1}{2}} \quad (21)$$

Where, V_{bb} is the potential at the boundary of the ZnO nanoparticles assumed to be 1 V, K_{ZnO} is the static dielectric constant of ZnO nanoparticles = 8.5, N_D is the donor density, roughly equal to the free carrier density of electrons in ZnO nanoparticle and e is the elementary charge of an electron. On surface modification of ZnO nanoplates, the dielectric constant will get modified according to Eq. 22, which will modify the surface band bending and the corresponding green emission.

The equivalent dielectric constant of the ZnO nanoplates immersed in the polymer PMMA/PVA can be calculated considering parallel dielectric constant formula:

$$K_{ZnO-polymer} = \frac{2k_1k_2}{k_1+k_2} \quad (22)$$

Where, k_1 is the dielectric constant of the ZnO, which is equal to 8.5 and k_2 is the dielectric constant of the polymers PVA or PMMA has values 3.2 and 3, respectively.

Table S5. The dielectric constant of ZnO and the surface-modified ZnO nanoplates

Samples name	Dielectric constant	Equivalent dielectric constant
1. ZnO	8.5 (ZnO)	8.50
2. ZPVA3	3.2 (PVA)	4.65
3. ZPMMA3	3.0 (PMMA)	4.43

From the table. S5 we see that the equivalent dielectric constant decreases on surface modification according to equation 22, hence the width of band bending according to equation 21. So, a decrease in green emission based on band bending theory is also expected to follow the trend ZPMMA3< ZPVA3 < ZnO, which matches the experimental observation.

References

[1] Foo et al., *Nanoscale Research Letters*, 2014, **9**, 429.
[2] S. Denchitcharoen, N. Siriphongsapak, P. Limsuwan, *Mater. Today: Proc.* 2017, **45**, 6146−6152.
[3] Ugochi Lydia Ifeanyichukwu et al., *Molecules*, 2020, **25**, 4521.
[4] H. D. Lutz, C. Jung, R. Mörtel, H. Jacobs, and R. Stahl, *Spectrochimica Acta Part A*, 1998, **54**, 7, 893–901.
[5] K. Demssie Dejen et al., *Rev. Adv. Mater. Sci.* 2020, **59**, 464–476.
[6] X-W Du et al., *Semicond. Sci. Technol.* 2006, **21**, 1202–1206.
[7] M S Tokumoto and V Briois, *J. Sol–gel Sci. Technol*., 2003, **26**, 547.
[8] Marco Laurenti et al., *Adv. Mater. Interfaces* 2017, ***4***, 1600758.
[9] O. Taratula, E. Galoppini, D. Wang, D. Chu, Z. Zhang, H. Chen, G. Saraf, Y. Lu, *J. Phys. Chem. B*, 2006, **110**, 6506.
[10] M. S. Lim, K. Feng, X. Chen, N. Wu, A. Raman, J. Nightingale, E. S. Gawalt, D. Korakakis, L. A. Hornak, A. T. Timperman, *Langmuir*, 2007, **23**, 2444.
[11] Marco Laurenti et al., *Adv. Mater. Interfaces*, 2017, **4**, 1600758
[12] L. Li, J. Dai, and E. Yamada. *Journal of Applied Polymer Science*, 2002, **86**, 2342–2347.
[13] Tannenbaum R, King S, Lecy J, Tirrell M and *L* Potts, *Langmuir*. 2004, **20**, 4507
[14] S. Jayswal, and R. S. Moirangthem, *New J. Chem.* 2018, **42**, 13689−13701.
[15] S. Sakohara, M. Ishida and M. A. Anderson, *J. Phys. Chem. B*, 1998, **102,** 10169.
[16] S Pandiarajan M, Umadevi, V Sasirekha, R K Rajaram and V Ramakrishnan, *J. Raman Spectrosc.* 2005, **36**, 950.
[17] Q. Li, *J. Membr. Sci.* 2017, ***544***, 68– 78.
[18] K. Vasuki, and R. Manimekalai, *Heliyon*, 2019, **5**, e02729.
[19] Sajid Ali Ansari, Mohammad Mansoob Khan, Shafeer Kalathil, Ambreen Nisar, Jintae Leea and Moo Hwan Cho, *Nanoscale***,** 2013, **5**, 9238-9246.
[20] Chun Hui Tan et al., *AIP Conference Proceedings*, 2016, **1784**, 040021.
[21] G.H. Schoenmakers et al., *J. Phys. Chem., 1996*, 100, 3215-3220.
[22] Nick S. Norberg, Daniel R. Gamelin, *J. Phys. Chem. B*, 2005, **44**, 109.
[23] R. Bhaskar et al., *Indian J Pure & Appl. Phys.*, 2009, **47**, 772-774.
[24] A. Hagfeldt, and G Michael, *Chem. Rev.* 1995, **95**, 49−68.
[25] H Moormann, D. Kohl, G. Heiland, *Surf. Sci.* 1980, **100**, 302−314.
[26] Yu Zhang et al., *J. Mater. Chem.*, 2012, **22**, 11971.
[27] C. A. Smith, H. W. H. Lee, V. J. Leppert, and S. H. Risbud, *Appl. Phys. Lett.* 1999, **75**, 1688.
[28] M. Kuno, J. K. Lee, B. O. Dabbousi, F. V. Mikulec, and M. G. Bawendi, *J. Chem. Phys.* 1997, **106**, 9869**.**
[29] T Chen, G Z Xing, Z Zhang, H Y Chen, T Wu, *Nanotechnology*, 2008, **19,** 435711.
[30] S. Vempati, J. Mitra and P. Dawson, *Nanoscale Res. Lett*., 2012, 7, 470.
[31] Sesha Vempati et al., *App. Phys. Lett.*, 2012, **100**, 162104**.**